The Adaptive Cross Approximation Algorithm for Accelerated Method of Moments Computations of EMC Problems

Kezhong Zhao, *Student Member, IEEE*, Marinos N. Vouvakis, *Student Member, IEEE*, and Jin-Fa Lee, *Fellow, IEEE*

***Abstract*—This paper presents the adaptive cross approximation (ACA) algorithm to reduce memory and CPU time overhead in the method of moments (MoM) solution of surface integral equations. The present algorithm is purely algebraic; hence, its formulation and implementation are integral equation kernel (Green's function) independent. The algorithm starts with a multilevel partitioning of the computational domain. The interactions of well-separated partitioning clusters are accounted through a rank-revealing LU decomposition. The acceleration and memory savings of ACA come from the partial assembly of the rank-deficient interaction submatrices. It has been demonstrated that the ACA algorithm results in $O(N\log N)$ complexity (where N is the number of unknowns) when applied to static and electrically small electromagnetic problems. In this paper the ACA algorithm is extended to electromagnetic compatibility-related problems of moderate electrical size. Specifically, the ACA algorithm is used to study compact-range ground planes and electromagnetic interference and shielding in vehicles. Through numerical experiments, it is concluded that for moderate electrical size problems the memory and CPU time requirements for the ACA algorithm scale as $N^{4/3}\log N$.**

***Index Terms*—Automotive electromagnetic compatibility (EMC), fast integral equation methods, infinite ground plane, method of moments (MoM).**

I. Introduction

THE method of moments (MoM) has been a very effective technique for modeling arbitrarily shaped antennas, scatterers, and electromagnetic compatibility (EMC) problems made of perfect electric conductors (PECs). Yet, the kernel of the integral equations, namely the Green's function, is a nonlocal operator. This results in a dense impedance matrix. Consequently, the storage, impedance matrix fill-in, and matrix-vector multiplication operations are of $O(N^2)$ complexity, where N is the number of unknowns.

A number of successful techniques have dramatically reduced memory and computational cost associated with the iterative solution of surface integral equations (SIEs). The exhausted list includes, but is not limited to, the fast multiple method (FMM) [1]–[5], the adaptive integral method (AIM) [6], [7], the precorrected fast Fourier transform (pFFT) method [8], and the panel clustering technique [9]. The multilevel FMM (MLFMM) [4], [5] has succeeded in reducing the numerical complexity of memory to $O(N)$ and CPU time to $O(N\log N)$. However, in the MLFMM algorithm, the formulation, implementation, and occasionally performance depend on *a priori* knowledge of the Green's function. The FFT-based methods, such as AIM and pFFT, replace the current basis functions by equivalent sources on a regular grid, which reproduce the same fields of the original current sources at some prescribed locations. Subsequently, for translational invariant kernels, the resulting impedance matrix has block Toeplitz structure; thus the evaluation of interactions can be accelerated through FFT. Certainly, near-field interactions are not accounted correctly by FFT and need to be corrected. The FFT-based methods work best on the volume integral equations (VIEs) and planar structures. For VIEs, the FFT-based methods achieve the complexity of $O(N\log N)$, whereas for SIEs, complexity is reduced to $O(N^{1.5})$ and $O(N^{1.5}\log N)$ for memory and CPU time, respectively. The panel clustering method, proposed by Hackbusch [9], works much like FMM, but instead of spherical wave expansion, the Green's function is approximated by the Taylor series. For non-oscillatory kernels, such as asymptotically smooth kernels, error bounds have been derived to rigorously choose the number of terms in the expansion. The complexity of the panel clustering method for static applications can be optimal.

The ACA algorithm [10], [11] presented herein takes advantage of the rank-deficient nature of the coupling matrix blocks representing well-separated MoM interactions. The algorithm was originally proposed by Bebendorf in [12]–[14]. The beauty of the ACA algorithm is its purely algebraic nature. Namely the computational speed-up is achieved through linear algebra manipulations of the impedance matrix, e.g., QR decomposition, singular value decomposition (SVD), LU decomposition, etc. Thus, ACA's development and implementation do not depend on the complete knowledge of the integral equation kernel, basis functions or the integral equation formulation itself. Moreover, due to its algebraic nature, ACA can be modular and very easily integrated into various MoM codes. In summary, the ACA algorithm is a multilevel matrix-partitioning scheme that achieves its computational reduction through a rank-revealing LU decomposition of the rank-deficient submatrices, representing well-separated interactions.

In [12]–[14], the algorithm has been successfully applied to static and low frequency applications, where the integral kernels are asymptotically smooth, with $O(N\log N)$ complexity. This paper applies the original algorithm of Bebendorf to electromagnetic wave problems of moderate electrical size.

Manuscript received October 11, 2004; revised June 13, 2005.

The authors are with the ElectroScience Laboratory, Electrical Engineering Department, The Ohio State University, Columbus, OH 43210 USA (e-mail: zhao.74@osu.edu; vouvakis.1@osu.edu; lee.1863@osu.edu).

Digital Object Identifier 10.1109/TEMC.2005.857898

More specifically, when the discretization size of $h \approx \lambda/7$ (where h is the mesh element length) is employed and for problems up to 500 000 Rao–Wilton–Glisson (RWG) [15] unknowns, the memory and CPU time requirements of the ACA algorithm roughly scale as $N^{4/3}\log N$. The algorithm produces very accurate results using only a fraction of what are needed by conventional MoM both in terms of memory and total CPU time.

The remainder of this paper is organized as follows. Section II describes the similarities and differences of the ACA algorithm over existing methods. For the sake of completeness, Section III briefly summarizes the formulation of the electrical field integral equation (EFIE) for PEC bodies. Various multilevel partitioning schemes for the integral equations have already been published in the literature, such as the multilevel FMM [4], [5] and the multilevel matrix decomposition algorithm [16]. The multilevel partitioning approach adopted in this paper is similar to the approaches of the afore-mentioned references; therefore, the multilevel partitioning detail will be omitted. Section IV is the core of this paper. A formal description of the algorithm is given in Sections IV-A–C, whereas Section IV-D gives a detailed description and discussions of ACA. Several numerical results, along with computational complexity studies are presented in Section V. Finally the paper concludes in Section VI.

II. Differences Over Existing Fast IE Methods

Methods like MLFMM, AIM, etc. can be classified as physics-based techniques, according to [6]. Compared with algebraic methods such as ACA, physics-based methods are more efficient in terms of both memory and CPU time. However their efficiency is sometimes achieved at the expense of generality. For example, the formulation and implementation of the free space FMM algorithm would require modifications when applied to layered media problems. Moreover, the similar arguments apply between low- and high-frequency applications. However, ACA and other algebraic integral equation (IE) methods are general and apply with only minor modifications to a large variety of applications, e.g., static, electrodynamic, layered media. Unfortunately, the computational effort and complexity still depend on the application.

A large number of fast integral equation algebraic methods have already been developed. To name a few, these include the multilevel matrix decomposition algorithm (MLMDA) [17]–[19], the multilevel QR decomposition [20], fast direct solver [21], IES^3 [22], predetermined interaction list oct-tree (PILOT) based QR algorithm [23], the multilevel UV decomposition [24], fast dual MGS block factorization [25], and single-level IE-QR algorithm [26]–[28]. MLMDA was originally proposed for two-dimensional geometries [16]. When applied to general three-dimensional problems, it is found that the algorithm is efficient only for planar or piecewise planar objects [17]. The multilevel QR and fast direct solver propose the compression of well-separated impedance submatrices through the Householder QR process and SVD [29], respectively. Both methods require complete knowledge of each impedance submatrix, which results in $O(N^2)$ operation counts, but reduced memory storage. IES^3 and PILOT-based QR algorithm target static and electrical small applications. The rank-revealing process of IES^3 is done through the help of so-called "statistically determined rank-map." PILOT-based QR algorithm improves on IES^3 by combining MLFMM's oct-tree partitioning scheme, partial QR factorization process, and an *ad hoc* look-up rank table. The multilevel UV decomposition factorizes the local impedance matrix into a product form. The determination of the rank is also done through a predetermined rank table, constructed based on the behavior of the Green's function itself. Single-level IE-QR along with its predecessor dual-MGS is inspired from IES^3 but is free of previous assumption about the kernel of the integral equation. Furthermore, it does not require construction of any rank map, and it is a true rank-revealing algorithm.

The ACA algorithm was originally developed for the asymptotically smooth kernels [12], which include particle interactions, Laplace/Poisson equations, etc. For electromagnetic wave propagation/radiation/scattering problems, the integral kernel is oscillatory and thus formally does not fit in the description of asymptotically smooth kernels. Consequently, in a strict sense, the ACA algorithm is not applicable to the electromagnetic wave applications. Nevertheless, the ACA algorithm is in essence rank-revealing LU decomposition [12], thus it inherits all the advantages of IE-QR but without the need of the computationally intense MGS process.

III. EFIE Formulation

Before describing the formulation, it is essential to introduce some notations adopted throughout this paper. Boldface capital letters will represent matrices unless otherwise specified. Boldface lowercase letters represent column/row vectors. The overhead arrows will be reserved for vector fields.

For the sake of completeness, we present the final form of the EFIE after the application of the Galerkin method [30]

$$\begin{aligned}&\text{Seek } \vec{J}(\vec{r}) \in \mathbf{H}^{-1/2}_{\mathrm{div}_D}(D) \text{ such that}\\ &k_o^2 \int_D \vec{\lambda}(\vec{r}) \cdot \int_D g(\vec{r};\vec{r}')\vec{J}(\vec{r}')\, ds'\, ds\\ &\quad - \int_D \nabla\cdot\vec{\lambda}(\vec{r}) \int_D g(\vec{r};\vec{r}')\nabla\cdot\vec{J}(\vec{r}')\, ds'\, ds\\ &\qquad = -\frac{jk_o}{Z_o}\int_D \vec{\lambda}(\vec{r})\cdot\vec{E}^{\mathrm{inc}}\, ds \;\forall \vec{\lambda}(\vec{r}) \in \mathbf{H}^{-1/2}_{\mathrm{div}_D}(D)\end{aligned} \tag{1}$$

where k_o is the free space wavenumber, Z_o is the free space intrinsic impedance, D is the problem domain, $\vec{E}^{\mathrm{inc}}$ is the incident electric field, $g(\vec{r};\vec{r}')$ is the integral kernel, $\vec{J}$ is the unknown surface currents, and $\vec{\lambda}$ is the testing function. Here vectors $\vec{r}$ and $\vec{r}'$ refer to the observation and source locations, respectively. The exact definition of the function space $\mathbf{H}^{-1/2}_{\mathrm{div}_D}(D)$ can

be found in [31]. In fact, the lowest order of the $\mathbf{H}_{\mathrm{div}_D}^{-1/2}(D)$ basis functions is the usual RWG basis function [31].

IV. The Adaptive Cross Approximation Algorithm

It is well known that the entire impedance matrix obtained from the application of MoM (EFIE) is neither singular nor rank deficient except at the internal resonances [32], [33]. However, because of the nature of the Green's function, the matrix consists of many numerically rank-deficient sub-blocks. Namely, the dense matrix blocks representing the interactions between two well-separated groups can be accurately represented by a much-reduced set of column vectors. With this insight in mind, the ACA algorithm starts by grouping, in a multilevel fashion, the basis functions into geometrically clustered groups, similar to [4], [13]. The grouping of basis functions consequently splits the impedance matrix into a collection of submatrix blocks of various sizes. The diagonal blocks, which correspond to self-group interactions, as well as matrix blocks resulting from the interactions of two touching groups, are to be computed via the conventional MoM approach. The numerically rank-deficient matrix blocks, corresponding to interactions of well-separated groups, will be efficiently compressed through the ACA algorithm. In the rest of this section, the detail of the algorithm is presented, followed with a more in-depth discussion of the algorithm. Note that details of the ACA analysis can be found in the original work of Bebendorf [12]–[14]. For the sake of completeness, some parts of that analysis are also presented herein.

A. Outline of the ACA Algorithm

Let the $m \times n$ rectangular matrix $\mathbf{Z}^{m\times n}$ represent the coupling between two well-separated groups in the MoM computation. The ACA algorithm aims to approximate $\mathbf{Z}^{m\times n}$ by $\tilde{\mathbf{Z}}^{m\times n}$. In particular, the ACA algorithm constructs the approximate matrix $\tilde{\mathbf{Z}}^{m\times n}$ through a product form. Namely,

$$\tilde{\mathbf{Z}}^{m\times n} = \mathbf{U}^{m\times r}\mathbf{V}^{r\times n} = \sum_{i=1}^{r} \mathbf{u}_i^{m\times 1}\mathbf{v}_i^{1\times n} \tag{2}$$

where r is the effective rank of the matrix $\mathbf{Z}^{m\times n}$, $\mathbf{U}^{m\times r}$ and $\mathbf{V}^{r\times n}$ are two dense rectangular matrices. The goal of ACA is to achieve

$$\|\mathbf{R}^{m\times n}\| = \|\mathbf{Z}^{m\times n} - \tilde{\mathbf{Z}}^{m\times n}\| \le \varepsilon\|\mathbf{Z}^{m\times n}\| \tag{3}$$

for a given tolerance ε, where $\mathbf{R}$ is termed as the error matrix. Note that in this paper $\|\cdot\|$ refers to the matrix Frobenus norm [29]. For the electromagnetic applications, the effective rank $r < \min(m,n)$. Therefore, instead of storing entire $m \times n$ entries, the algorithm only requires to store $(m+n)\times r$ entries.

B. Notations

Before proceeding to the formal description of the ACA algorithm, it would be beneficial to define some notations. Let $\mathbf{I} = [I_1 \ \ldots \ I_r]$ and $\mathbf{J} = [J_1 \ \ldots \ J_r]$ be the arrays containing orderly selected row and column indexes of the matrix $\mathbf{Z}^{m\times n}$. $\mathbf{u}_k$ is kth column of the matrix $\mathbf{U}$ and $\mathbf{v}_k$ is kth row of the matrix $\mathbf{V}$. The algorithm is written in Matlab's notation, where $\tilde{\mathbf{R}}(I_1,:)$ stands for (I_1)th row of the matrix $\tilde{\mathbf{R}}$. $\tilde{\mathbf{Z}}^{(k)}$ is the matrix $\tilde{\mathbf{Z}}$ at kth iteration.

C. Detail of the ACA Algorithm

Below is the description of the ACA algorithm.

Initialization:

1) Initialize the 1st row index $I_1 = 1$ and set $\tilde{\mathbf{Z}} = 0$.
2) Initialize the 1st row of the approximate error matrix: $\tilde{\mathbf{R}}(I_1,:) = \mathbf{Z}(I_1,:)$.
3) Find the 1st column index $J_1 : |\tilde{\mathbf{R}}(I_1,J_1)| = \max_j(|\tilde{\mathbf{R}}(I_1,j)|)$.
4) $\mathbf{v}_1 = \tilde{\mathbf{R}}(I_1,:)/\tilde{\mathbf{R}}(I_1,J_1)$.
5) Initialize the 1st column of the approximate error matrix: $\tilde{\mathbf{R}}(:,J_1) = \mathbf{Z}(:,J_1)$.
6) $\mathbf{u}_1 = \tilde{\mathbf{R}}(:,J_1)$.
7) $\|\tilde{\mathbf{Z}}^{(1)}\|^2 = \|\tilde{\mathbf{Z}}^{(0)}\|^2 + \|\mathbf{u}_1\|^2\|\mathbf{v}_1\|^2$.
8) Find 2nd row index $I_2 : |\tilde{\mathbf{R}}(I_2,J_1)| = \max_i(|\tilde{\mathbf{R}}(i,J_1)|), i \ne I_1$.

kth Iteration:

1) Update (I_k)th row of the approximate error matrix: $\tilde{\mathbf{R}}(I_k,:) = \mathbf{Z}(I_k,:) - \sum_{l=1}^{k-1}(\mathbf{u}_l)_{I_k}\mathbf{v}_l$.
2) Find kth column index $J_k : |\tilde{\mathbf{R}}(I_k,J_k)| = \max_j(|\tilde{\mathbf{R}}(I_k,j)|), j \ne J_1,\ldots,J_{k-1}$.
3) $\mathbf{v}_k = \tilde{\mathbf{R}}(I_k,:)/\tilde{\mathbf{R}}(I_k,J_k)$.
4) Update (J_k)th column of the approximate error matrix: $\tilde{\mathbf{R}}(:,J_k) = \mathbf{Z}(:,J_k) - \sum_{l=1}^{k-1}(\mathbf{v}_l)_{J_k}\mathbf{u}_l$.
5) $\mathbf{u}_k = \tilde{\mathbf{R}}(:,J_k)$.
6) $\|\tilde{\mathbf{Z}}^{(k)}\|^2 = \|\tilde{\mathbf{Z}}^{(k-1)}\|^2 + 2\sum_{j=1}^{k-1}|\mathbf{u}_j^T\mathbf{u}_k|\cdot|\mathbf{v}_j^T\mathbf{v}_k| + \|\mathbf{u}_k\|^2\|\mathbf{v}_k\|^2$.
7) Check convergence: If $\|\mathbf{u}_k\|\|\mathbf{v}_k\| \le \varepsilon\|\tilde{\mathbf{Z}}^{(k)}\|$, end iteration.
8) Find next row index $I_{k+1} : |\tilde{\mathbf{R}}(I_{k+1},J_k)| = \max_i(|\tilde{\mathbf{R}}(i,J_k)|), i \ne I_1,\ldots,I_k$.

Note that this algorithm approximates the original matrix by requiring only *partial* knowledge of the original matrix. The above procedure requires $O(r(m+n))$ memory storage. Because steps 1 and 4 of k th iteration require $O(r(m+n))$ operations for each iteration, and there are total r iterations, CPU time scales as $O(r^2(m+n))$.

D. Discussion

To understand the ACA algorithm further, the true error matrix $\mathbf{R}^{(k)} = \mathbf{Z} - \tilde{\mathbf{Z}}^{(k-1)}$ is to be examined, where $\tilde{\mathbf{Z}}^{(k-1)} = \mathbf{U}^{m\times(k-1)}\mathbf{V}^{(k-1)\times n} = \sum_{i=1}^{k-1}\mathbf{u}_i^{m\times 1}\mathbf{v}_i^{1\times n}$ is the rank$(k-1)$ approximate matrix at $(k-1)$th iteration. Note that from this point on, the superscripts describing the matrix dimensions are often omitted either when the dimensions are not relevant to the discussion or when they are obvious. Denote $\mathbf{e}_{i,n}$ as ith column of an identity matrix $\mathbf{I}^{n\times n}$ and $\mathbf{e}_{i,m}^T$ ith row of $\mathbf{I}^{m\times m}$. Initially, at $k=0$, we have $\tilde{\mathbf{Z}}^{(0)} = 0$ and $\mathbf{R}^{(1)} = \mathbf{Z} - \tilde{\mathbf{Z}}^{(0)} = \mathbf{Z}$. The update of the approximate matrix $\tilde{\mathbf{Z}}$ continues by following the ACA algorithm. At kth iteration, with the row and column indexes, I_k and J_k, respectively selected, it can be shown

that [12]

$$\mathbf{R}^{(k)} = \mathbf{R}^{(k-1)} - \gamma_{k-1}\mathbf{R}^{(k-1)}\mathbf{e}_{J_{k-1},n}\mathbf{e}^T_{I_{k-1},m}\mathbf{R}^{(k-1)}$$

$$\gamma_{k-1} = \frac{1}{\mathbf{R}^{(k-1)}(I_{k-1}, J_{k-1})}. \quad (4)$$

Subsequently, the new column and row vectors are computed via

$$\mathbf{u}_k = \mathbf{R}^{(k)}\mathbf{e}_{J_{k,n}} \quad (5)$$

$$\mathbf{v}_k = \gamma_k \mathbf{e}^T_{I_{k,m}}\mathbf{R}^{(k)}. \quad (6)$$

Moreover, the rank (k) approximate matrix at kth iteration is expressed as [12]

$$\tilde{\mathbf{Z}}^{(k)} = \tilde{\mathbf{Z}}^{(k-1)} + \gamma_k \mathbf{R}^{(k)}\mathbf{e}_{J_k,n}\mathbf{e}^T_{I_k,m}\mathbf{R}^{(k)}. \quad (7)$$

One important fact to realize is that the entries of (I_k)th row and (J_k)th column of the error matrix at $(k+1)$th iteration

$$\mathbf{R}^{(k+1)}(I_k,:) = \mathbf{R}^{(k)}(I_k,:) - \mathbf{R}^{(k)}(I_k, J_k)\cdot\frac{\mathbf{R}^{(k)}(I_k,:)}{\mathbf{R}^{(k)}(I_k, J_k)} = \mathbf{0} \quad (8)$$

$$\mathbf{R}^{(k+1)}(:, J_k) = \mathbf{R}^{(k)}(:, J_k) - 1\cdot\mathbf{R}^{(k)}(:, J_k) = \mathbf{0}. \quad (9)$$

This means that the product $\mathbf{u}_k \cdot \mathbf{v}_k$ exactly reproduces the original entries of (I_k)th row and (J_k)th column of the true error matrix $\mathbf{R}^{(k)}$. Consequently, the product $\mathbf{u}_1 \cdot \mathbf{v}_1$ exactly recovers (I_1)th row and (J_1)th column of the original matrix $\mathbf{Z}^{m\times n}$, whereas $\mathbf{u}_2 \cdot \mathbf{v}_2$ combined with $\mathbf{u}_1 \cdot \mathbf{v}_1$ exactly retrieve (I_2)th row and (J_2)th column. This process continues *adaptively* until the condition $\|\mathbf{R}^{(k)}\| \le \varepsilon\|\mathbf{Z}^{(k)}\|$ is satisfied, which declares the convergence of the algorithm.

If no pivoting is performed, namely if we set $I_k = k$ and $J_k = k$, the error matrix would take the form [12]

$$\mathbf{R}^{(k)} = \begin{bmatrix} 0 & \dots & 0 & 0 & 0 & \dots & 0 \\ \vdots & \ddots & \vdots & \vdots & \vdots & \ddots & \vdots \\ 0 & \dots & 0 & 0 & 0 & \dots & 0 \\ 0 & \dots & 0 & \mathrm{X} & \dots & & \mathrm{X} \\ 0 & \dots & 0 & \vdots & & & \\ \vdots & \ddots & \vdots & & & & \\ 0 & \dots & 0 & \mathrm{X} & & & \end{bmatrix} \quad (10)$$

where the row and column marked with X are kth row and kth column, respectively. From (5) and (6), we have

$$\mathbf{u}_k = \begin{bmatrix} 0 \\ \vdots \\ 0 \\ \mathbf{R}^{(k)}(k,k) \\ \mathbf{R}^{(k)}(k+1,k) \\ \vdots \\ \mathbf{R}^{(k)}(m,k) \end{bmatrix}$$

$$\mathbf{v}_k = \begin{bmatrix} 0 & \dots & 0 & 1 & \dfrac{\mathbf{R}^{(k)}(k,k+1)}{\mathbf{R}^{(k)}(k,k)} & \dots & \dfrac{\mathbf{R}^{(k)}(k,n)}{\mathbf{R}^{(k)}(k,k)} \end{bmatrix}. \quad (11)$$

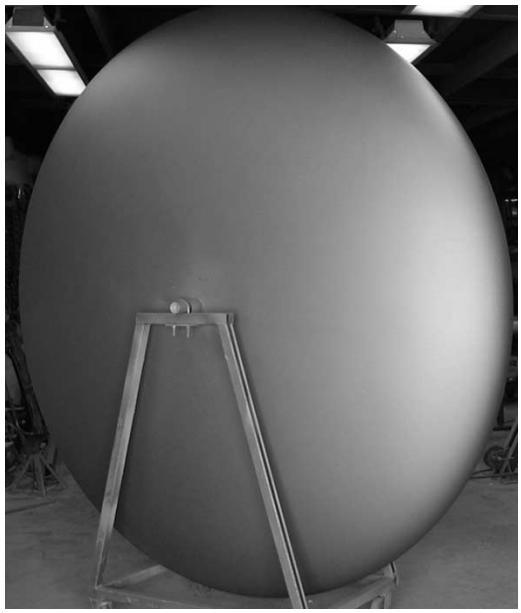

Fig. 1. The picture of the blended surface ground plane. The ground plane is designed to mimic the performance of an infinite ground plane.

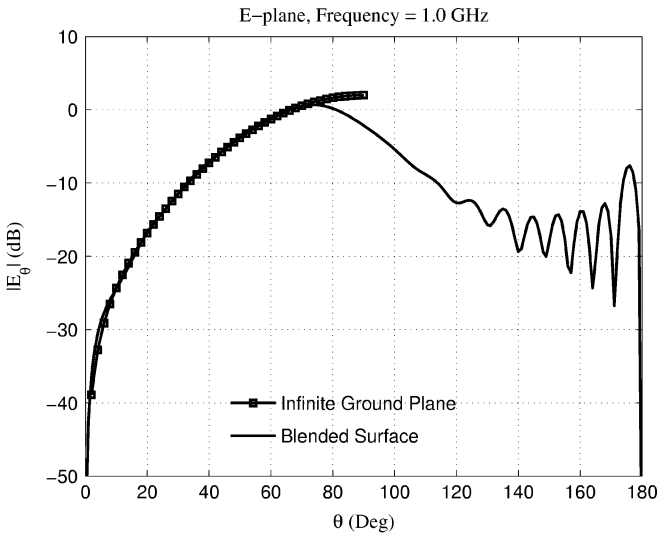

Fig. 2. E-plane radiation patterns of a vertical infinitesimal electrical dipole in the presence of the blended surface and an infinite ground plane.

If the matrix $\mathbf{Z}^{m\times n}$ is full rank, that is, $r = \min(m, n)$, then $\mathbf{U}^{m\times r} = [\mathbf{u}_1 \ \dots \ \mathbf{u}_r]$ is a lower triangular matrix and $\mathbf{V}^{r\times n} = \begin{bmatrix} \mathbf{v}_1 \\ \vdots \\ \mathbf{v}_r \end{bmatrix}$ is a unit upper triangular matrix. This fact reveals that the ACA algorithm is very similar to the column pivoted LU decomposition [12].

E. Error Definition

The ACA algorithm terminates when $\|\mathbf{R}^{(k)}\| \le \varepsilon\|\mathbf{Z}\|$, with a specified tolerance ε. However, the exact computations of $\|\mathbf{R}^{(k)}\|$ and $\|\mathbf{Z}\|$ require complete knowledge of $\mathbf{Z}$. To facilitate an efficient implementation, a way to compute $\|\mathbf{R}^{(k)}\|$ approximately is needed. This is done by considering kth row

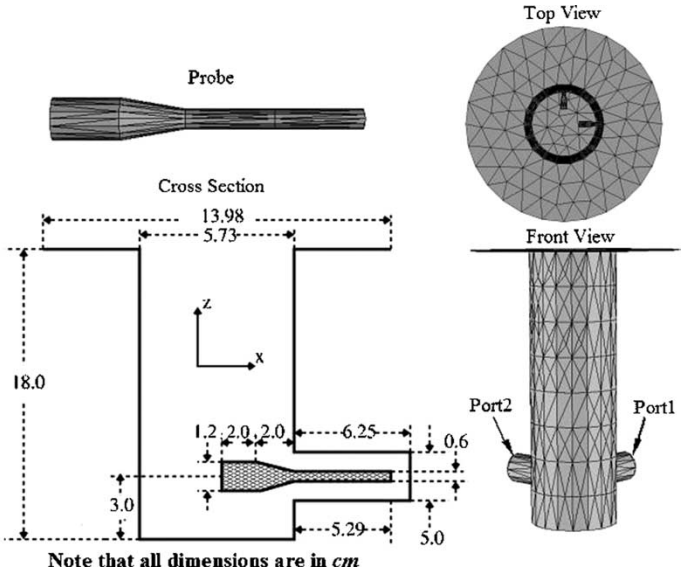

Fig. 3. Views and dimensions of the cylindrical waveguide aperture radiator along with the excitation probes.

and column as the most dominant row and column of $\mathbf{R}^{(k)}$, respectively. Namely,

$$\|\mathbf{R}^{(k)}\| = \|\mathbf{Z} - \tilde{\mathbf{Z}}^{(k-1)}\| \approx \|\mathbf{u}_k\| \cdot \|\mathbf{v}_k\|. \tag{12}$$

Similarly, $\|\mathbf{Z}\|$ can be well approximated by $\|\tilde{\mathbf{Z}}^{(k)}\| = \|\mathbf{U}^{(k)} \cdot \mathbf{V}^{(k)}\|$.

V. Numerical Results

This section accesses the accuracy aspects and numerical complexity of the ACA algorithm for a number of EMC-related applications. All the computations were carried out on an AMD 64-bit Opteron Workstation with 16 GB RAM and ACA terminating tolerance $\varepsilon = 10^{-3}$ was used, unless otherwise specified. All the computations were done in single precision arithmetic. The resulting impedance matrices were iteratively solved using the GMRES (60) solver [34], where 60 is the restart number. The convergence of the iterative solution process was accelerated with the use of the "geo-neighboring" preconditioner reported in [35]. Note that Bebendorf has proposed a preconditioner [36] that is spectrally equivalent to the approximated matrix by the ACA algorithm and can be computed purely algebraically with the same order of complexity as the ACA algorithm.

A. Accuracy

1) Finite Ground Plane: Measurements in the presence of a ground plane are very common in EMI/EMC community. When determining the limits for radio frequency (RF) emission from electronic products, the measurements are required to be performed on an ideal open area test site (OATS), namely, a perfectly conducting infinite ground plane [37]. In this first example, the ACA algorithm is used to study a finite ground plane design [38], whose purpose is to mimic the performance of an infinite ground plane on a compact range environment. The ground plane will be referred to as the blended surface throughout the paper. The blended surface is a body of revolution as shown in Fig. 1 and is described by the following equations:

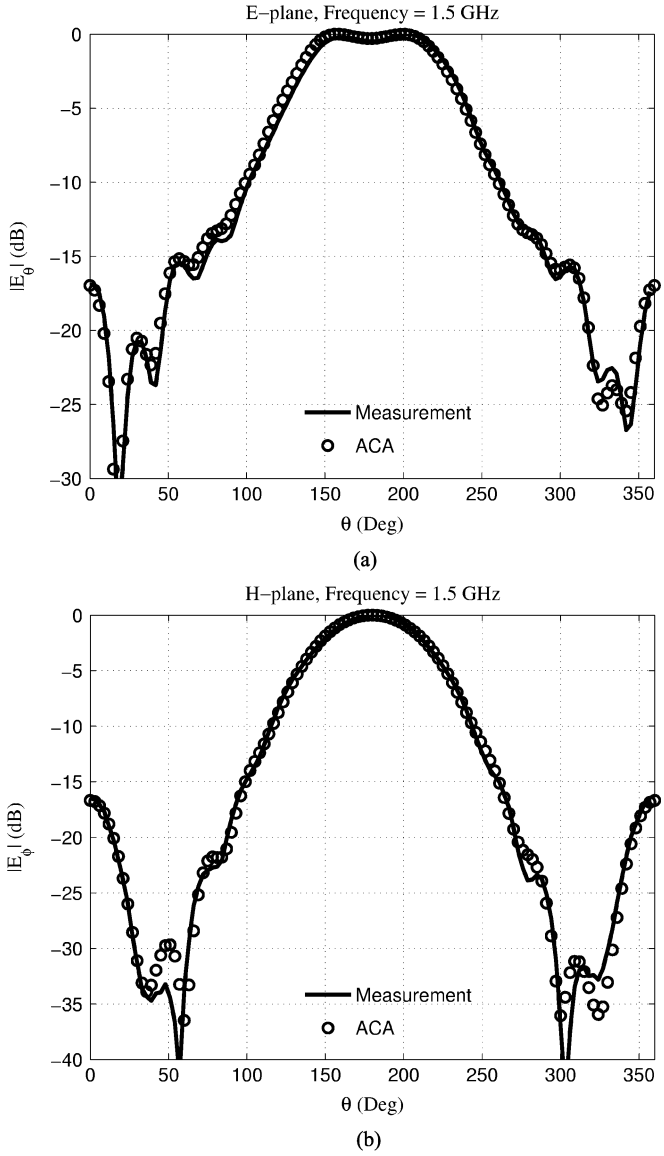

Fig. 4. Radiation patterns of the cylindrical waveguide without ground plane, only one port being excited. (a) E-plane and (b) H-plane.

For $0 \le \phi \le 360^\circ$

$$\rho = \frac{x_{\max}}{\gamma_{\max}}\gamma(1 - b(\gamma)) + b_e \sin(\gamma) b(\gamma), \quad 0 \le \gamma \le 150^\circ$$

$$z = (a_e \cos(\gamma) - a_e) b(\gamma) \tag{13}$$

where $\gamma_{\max} = 150^\circ, x_{\max} = 180$ cm, $a_e = 27.56$ cm, $b_e = 121.85$ cm, and

$$b(\gamma) = \frac{1}{2}\left(1 - \cos\left(\frac{\pi\gamma}{\gamma_{\max}}\right)\right). \tag{14}$$

For these parameters the diameter of the ground plane is approximately 2.4 m and the height is 0.5 m.

To show that the blended surface does mimic the performance of the infinite ground plane, the ground plane is excited with a vertical infinitesimal electric current source. The infinitesimal

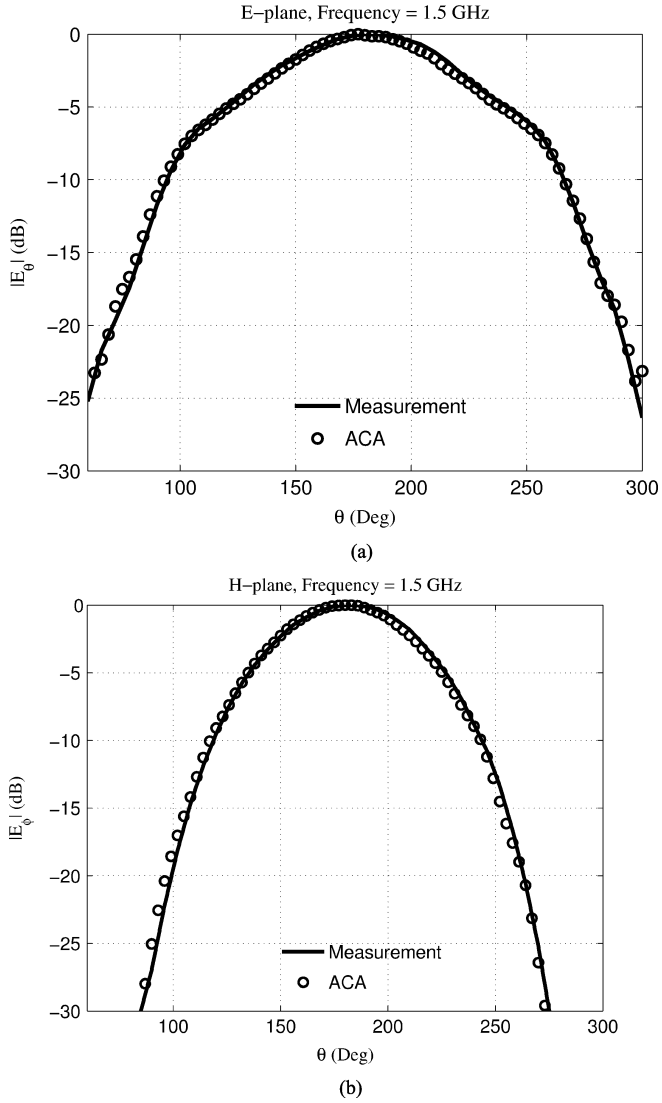

Fig. 5. Radiation patterns of the cylindrical waveguide mounted on the blended surface, only one port being excited. (a) E-plane and (b) H-plane.

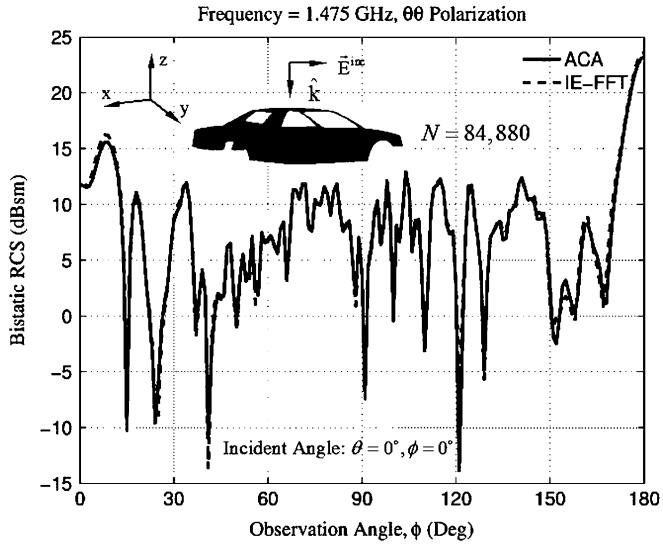

Fig. 6. Bistatic scattering pattern of a realistic car at 1.475 GHz. The plane wave is incident at $\theta = 0^\circ, \phi = 0^\circ$ (toward top of the car). The car is modeled using 84 880 RWG unknowns.

electric current source here is modeled by a dipole of length 0.1 cm, with constant current $I_o = 1.0$. The current source is located 6.25 cm vertically above the center of the ground plane, which is a quarter wavelength long at the testing frequency of 1.0 GHz. The resulting radiation pattern is compared with the analytical solution [39]. Fig. 2 shows the comparison of the performances of the blended surface and the infinite ground plane. It is observed that the magnitude of the antenna pattern for the blended surface is very smooth, due to the elimination of any diffraction centers, and agrees very closely to the infinite ground plane result up to about 80°. Notice that in the backward direction, a lot of ripples are observed predominately due to the creeping waves on the blend surface. In addition, the phase pattern, not shown herein because of space limitations, exhibits similar characteristics.

Because the excitation by an infinitesimal source is not a practical one, a cylindrical waveguide with two circular polarized port arrangements is considered. Fig. 3 illustrates the geometry and dimensions of the waveguide along with the locations of the excitation probes. The waveguide is excited by activating the horizontal probe (the probe along x-axis) while shorting out the other probe. The simulated results of the ACA algorithm are compared with the measurements at the testing frequency of 1.5 GHz, as shown in Fig. 4, where very good agreement between ACA and measured results is observed. In this example, there is a side lobe on the back and the E-plane pattern is not quite smooth. This is mainly due to edge diffraction from the top circular plate, which reveals that the flat plate is not a good substitute for the infinite ground plane.

The circular waveguide is then mounted on the blended surface operated under the same frequency. The comparison of simulated results with the measured data is shown in Fig. 5. In this case, the side lobe is completely eliminated and the patterns are much smoother. Simulated results agree very well with the measurements. Moreover, through the antenna patterns, of both the measurements and the simulations, it is confirmed that the blended surface is a very practical approximation to the infinite ground plane for antenna measurements.

2) Vehicular Platform: To further validate accuracy of the ACA algorithm, the shielding effect of a vehicular platform in the presence of an incident plane wave is studied. First, the bistatic radar cross section (RCS) of a simplified Pontiac GrandAm chassis is computed, and the result is compared with an existing IE code. The mesh of the vehicle is shown in the insert of Fig. 6. The dimensions of the vehicle are about 5.1 m × 1.9 m × 1.2 m along the x-, y-, and z-direction, respectively. For the bistatic RCS computation, the vehicle is excited by a θ-polarized plane wave incident from the top $(\theta = 0^\circ, \phi = 0^\circ)$ with $f = 1.475$ GHz. The problem is modeled using 84 880 RWG unknowns, and requires 1.6 GB of memory. Fig. 6 also shows the RCS pattern, and the ACA result agrees well with that of IE-FFT [41].

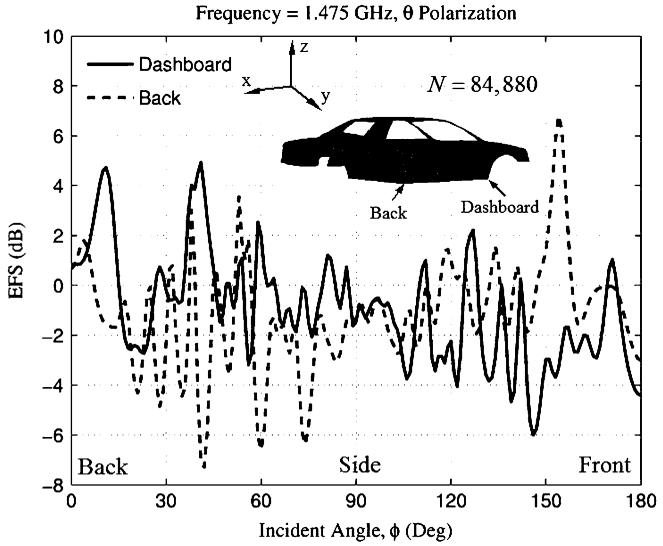

(a)

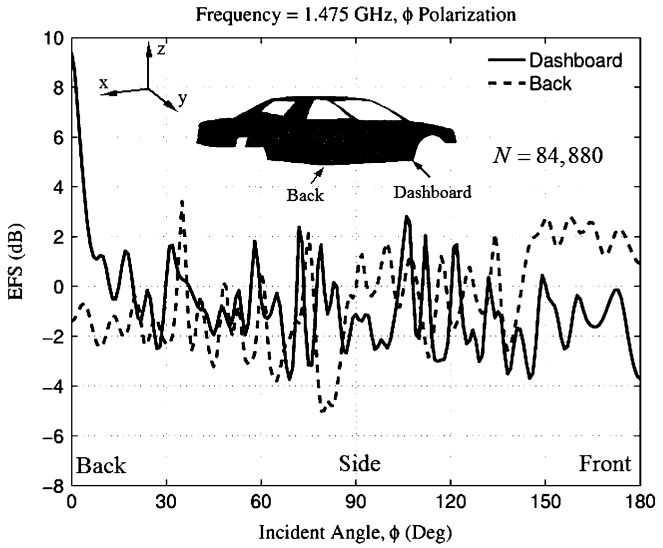

(b)

Fig. 7. EFS evaluated at two locations for various incident waves. The locations are specified in the figure.

Next, the electromagnetic interference and shielding are studied. In this scenario, the shielding effectiveness of the car platform is assessed when it is impinged with a monochromatic plane wave coming from possibly a radar or a cellular base station. The near-fields at some locations inside the vehicle are evaluated. The electric field shielding (EFS) of this vehicle defined by [40]

$$\mathrm{EFS}(\vec{r}) = -20\log\left(\frac{\left|\vec{E}^{\mathrm{total}}(\vec{r})\right|}{\left|\vec{E}^{\mathrm{inc}}(\vec{r})\right|}\right)\ \mathrm{dB} \qquad (15)$$

is evaluated at two locations, $\vec{r}$: one at back of the car and the other at the dashboard (see Fig. 7). Both locations are along the x-axis, namely, $\vec{r} = (x, y, z) = (2.15, 0, 0.75)$ and $\vec{r} = (x, y, z) = (4.2, 0, 0.75)$. The vehicle is illuminated by

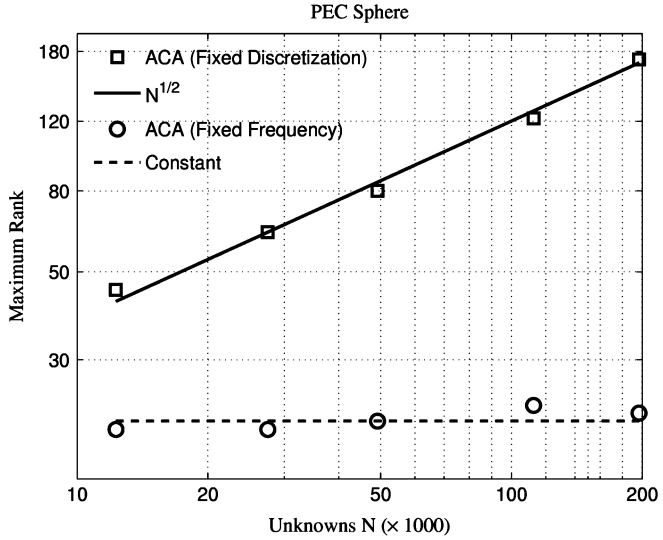

Fig. 8. Behavior of maximum rank for a PEC sphere example. Two cases are studied: (1) fixed discretization and increasing frequency; (2) fixed frequency and decreasing discretization.

plane waves coming from all possible directions in xy plane, and both θ and ϕ polarizations are considered. In Fig. 7 the computed EFS for both horizontal and vertically polarized incident waves are shown. Notice that for $\phi = 0^\circ$ (incidence from the back of the car) the dashboard is the most visible and consequently has higher EFS. Similarly, EFS is higher at the back for incident wave coming from about $\phi = 180^\circ$.

B. Performance

Having established the confidence in the accuracy of the ACA algorithm on fairly realistic problems, in this section the computational features of the ACA algorithm are explored. In EM computations, two types of numerical complexity result can be reported. One occurs when the number of unknowns increases just by discretizing the geometry to a finer and finer level, at a fixed frequency. This is the situation encountered in geometrically complicated problems that exhibit field singularities. The other one is encountered when the number of unknowns increases by retaining a specific discretization size h, in terms of wavelength, and increasing the frequency or increase the dimension. This situation is encountered when electrically large problems are to be solved.

1) Fixed Frequency, Varying Discretization Sizes: The first experiment performed is using a PEC sphere of radius of $1m$ as the example and fixing the frequency to be 30 MHz, and decreasing the discretization size h from $\lambda/130$ to $\lambda/520$. Subsequently, the number of unknowns N increases simply because smaller discretization is employed for better accuracy, assuming stable integral equation methods are adopted, see [35]. This situation is analogous to study the ACA algorithm for electrically small problems, namely, static and low-frequency limit applications. Assuming that each submatrix has rank r, the asymptotic complexity of $O(r^2 N \log N)$ is required to perform the ACA algorithm and $O(rN\log N)$ to store the matrix [14].

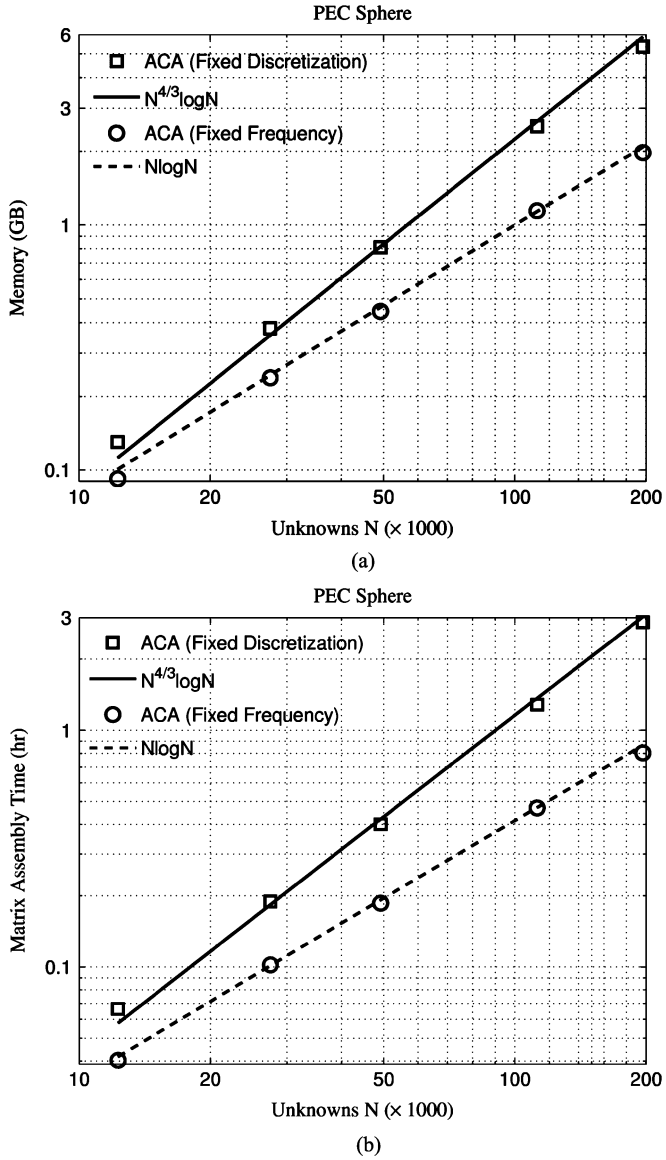

Fig. 9. Complexity of the ACA algorithm for a PEC sphere example; (a) memory, (b) CPU time. Two experiments are performed: (1) fixed discretization and increasing frequency; (2) fixed frequency and decreasing discretization.

From the doctrine of FMM, it is expected the maximum rank $r_{\max} \propto (ka)^2$, where k is wavenumber and a is the diameter of the smallest sphere enclosing the largest group. Since frequency is fixed, $(ka)^2$ is constant. Therefore, $r_{\max}$ should approach to constant, which is indeed the case as shown in Fig. 8. Consequently, the complexity for both memory consumption and CPU time is $O(N\log N)$, as can be seen from Fig. 9.

2) Fixed Discretization, $(h/\lambda = \text{const.})$, Varying the Frequencies: In this case, the performance of the ACA algorithm is studied for electrically increasing large problems. Namely, for the same PEC sphere example, with $h/\lambda = 1/7$, and the frequency is increased from 600 MHz to 2.4 GHz. Subsequently, from geometrical consideration, the relation $n \propto k^2a^2$ holds, where n is the number of unknowns in a specific group and a is the diameter of the smallest sphere enclosing the largest group. By FMM theory, $r_{\max}$ should follow $r_{\max} \propto N$, where N is the total number of unknowns. However, through numerical experiments, it is found that $r_{\max}$ grows as $O(N^{0.5})$ as indicated in Fig. 8, and moreover, the majority of the rank distribution remains unchanged with frequency as shown in Fig. 10. This is because the examples only of medium electrical sizes are conducted and the sampling limits have not been encountered yet. This observation is further confirmed when the exact SVD is performed on the coupling matrices resulting from two well-separated groups (in this case, two spheres of radius of $1m$). As indicated by Fig. 11 the dominant singular values also grow as $O(N^{0.5})$ when $\varepsilon = 10^{-3}$. Term the submatrices whose ranks are close to $r_{\max}$ the dominant submatrices. For these dominant submatrices the memory requirement is $O(N^{1.5})$ and CPU time requires $O(N^2)$. Nevertheless, these submatrices consist of very low percentage of overall submatrices, and the majority of submatrices have complexity proportional to $N^{4/3}\log N$ for both memory storage and matrix assembly time. The above conclusions are also suggested in Fig. 9. The complexity of dominant sub-matrices will not dominate overall ACA process until some high number of unknowns is reached (in this example which is approximately 500 000 unknowns).

Therefore, it could be concluded that the complexity for the ACA algorithm for wave propagation application, scales as $N^{4/3}\log N$ for *practical* moderate sized problems, even though it could be proportional to $N^{1.5}$ and N^2 for memory and CPU time, respectively. It should be emphasized that, asymptotically as $N \to \infty$, the complexity of the ACA algorithm could be scaled as poor as $O(N^2)$ and $O(N^3)$ for memory and CPU time, respectively. However, we should remark here that these theoretical complexities should not be taken literally as to conclude that the ACA algorithm is not effective in speeding up MoM computations. On the contrary, for many practical applications, with moderate electrical sizes, it is found that the ACA algorithm outperforms FMM, particularly with multiple right-hand-side excitations.

C. ACA versus IE-QR

To show the kernel independent nature of the ACA algorithm, a number of corporate-fed planar microstrip antenna array examples are analyzed. The analysis requires the use of the layered media Green's function. The details in the geometry and the dimensions of all microstrip structures used in this section can be found in [42]. To evaluate the accuracy and error control of the ACA algorithm let's first define the root mean square (rms) error of far-field as

$$\eta = \frac{\sqrt{\int_0^{2\pi}\int_0^{\pi} \left|\sum_{\text{mom}}(\theta,\phi) - \sum_{\text{aca}}(\theta,\phi)\right|^2 \sin\theta\, d\theta\, d\phi}}{\sqrt{\int_0^{2\pi}\int_0^{\pi} \left|\sum_{\text{mom}}(\theta,\phi)\right|^2 \sin\theta\, d\theta\, d\phi}} \tag{16}$$

where θ and ϕ are angles of observation points, and $\sum_{\text{mom}}(\theta,\phi), \sum_{\text{aca}}(\theta,\phi)$ are far-fields computed by traditional MoM and ACA approaches, respectively. Fig. 12 shows far field rms error with varying ACA tolerance. In this study a 8×8

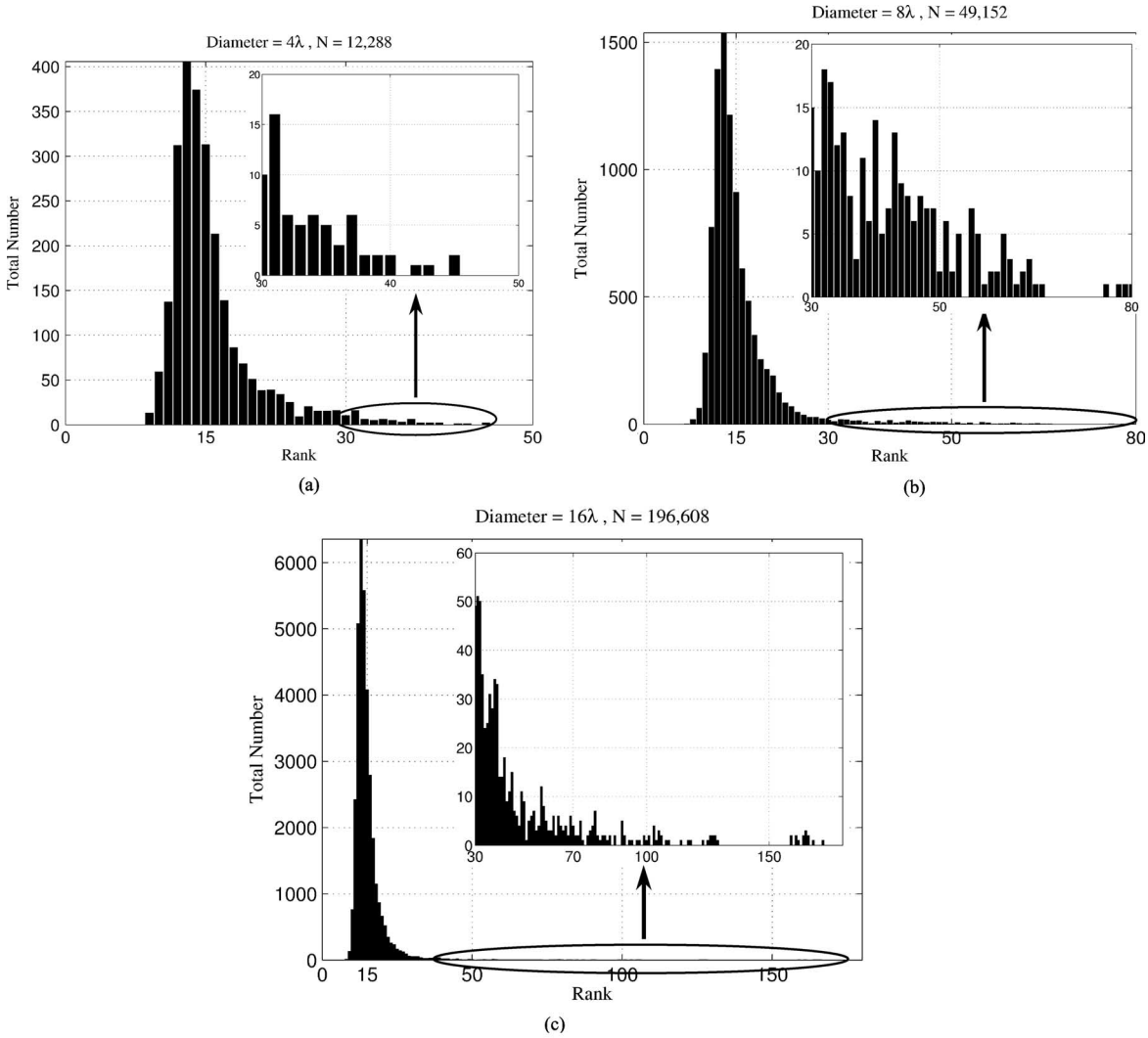

Fig. 10. Rank distributions of the ACA sub-matrices when applied to a PEC sphere example at various frequencies with fixed discretization, (a) 600 MHz. (b) 1.2 GHz. (c) 2.4 GHz.

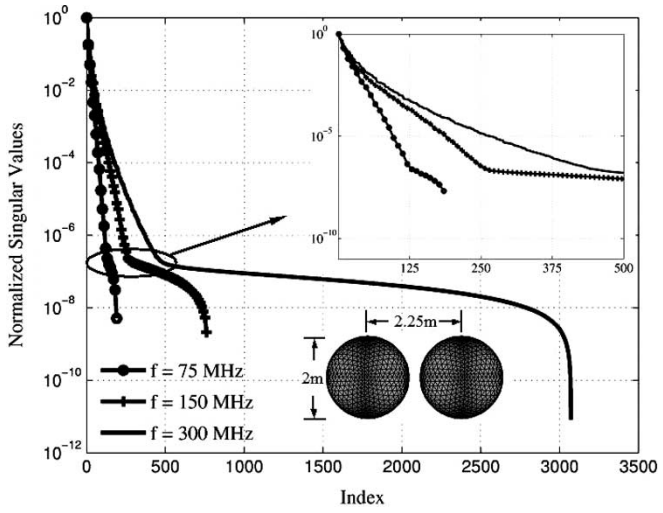

Fig. 11. Normalized singular values of the coupling matrices of two nontouching PEC spheres. The coupling matrices are computed through the traditional MoM approach at three different frequencies with fixed discretization. The singular values are normalized to the largest one.

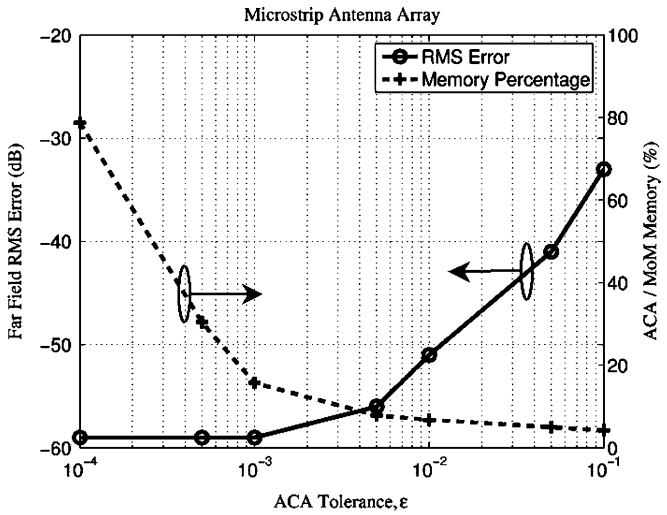

Fig. 12. Far-field rms error and ratio between memory for ACA and memory for MoM as a function of ACA terminating tolerance ε. The study is performed with a 8×8 corporate-fed microstrip array.

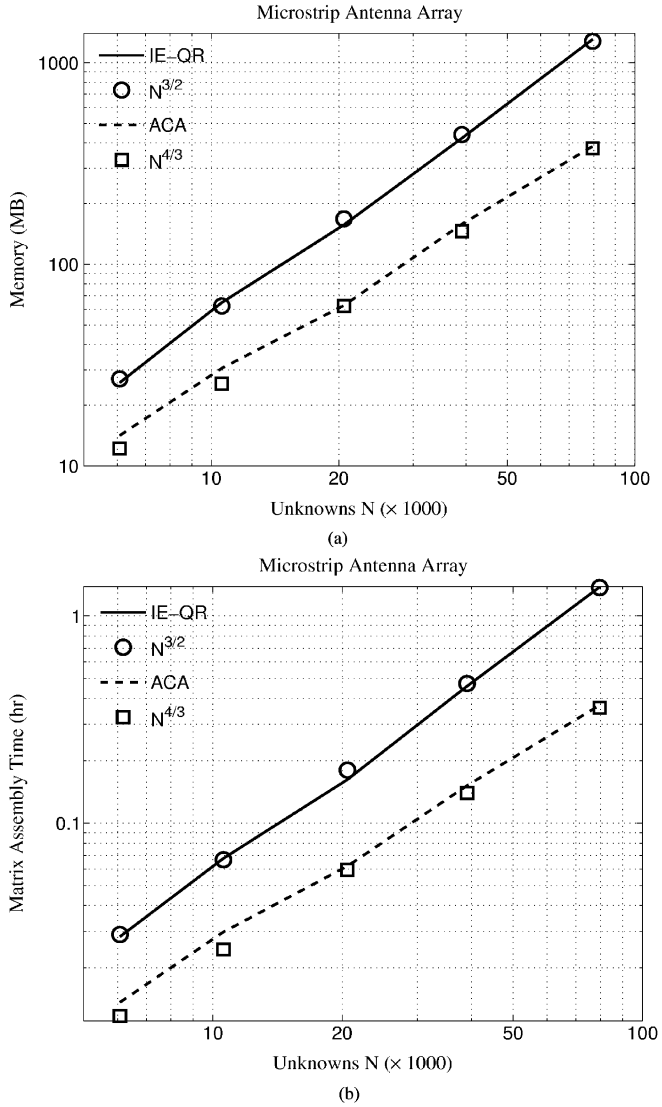

Fig. 13. Comparisons of the complexity between ACA and single-level IE-QR algorithms for layered medium application. (a) Memory. (b) CPU time. All the computations were performed on a Pentium IV 1.8 GHz with 2 GB RAM PC.

corporate-fed array is used. Note that for an ACA tolerance of 10^{-2} a very accurate result can be achieved.

To show that ACA offers a better alternative than single-level IE-QR, complexities are compared with tolerance $\varepsilon = 10^{-2}$ for both ACA and single-level IE-QR. For this application, all the computations were performed on a Pentium IV 1.8 GHz with 2 GB RAM PC. In this case, the frequency is fixed at 9.42 GHz, but the dimensions of array increase from 8×4 to 32×32. ACA outperforms single-level IE-QR, both in terms of proportionality constant and complexity scaling as shown in Fig. 13.

VI. Conclusion

In this paper, the ACA algorithm is extended to wave propagation problems. The algorithm is independent of Green's functions and effectively compresses the impedance matrix as data sparse representation and thus accelerates the matrix assembly computation as well as matrix vector multiplication. It is revealed that the algorithm is very similar to column-pivoted LU decomposition. Through numerical computations, it is found that the ACA algorithm is very stable and produces very accurate results, making the algorithm a very effective and reliable computer-modeling tool. Through some extensive performance studies, the complexity of $O(N\log N)$ is fully recovered at the low-frequency limit, and at the moderate-frequency ranges, the computational overhead scales as $N^{4/3}\log N$ for both memory and CPU time requirements, even though in theory it could be $O(N^2)$ for memory requirement and $O(N^3)$ for CPU time.

Acknowledgment

The authors would like to thank the anonymous reviewers for their constructive comments and suggestions. Many useful corrections were provided by Dr. I. J. Gupta, who also provided the opportunity for the study of the ground plane. The authors thank Dr. C.-C. Chen for the geometry and measurement data of cylindrical waveguide. The authors appreciate the help of Dr. K. Sertel for providing the triangular mesh of the car model. The authors are grateful to S. M. Seo for helpful discussions, and the help on the quality improvement on the figures in this transcript, and for provision of the reference result of IE-FFT.

References

[1] V. Rokhlin, "Rapid solution of integral equations of classic potential theory," *J. Comput. Phys.*, vol. 60, no. 1, pp. 187–207, 1985.
[2] V. Rokhlin, "Rapid solution of integral equations of scattering in two dimensions," *J. Comput. Phys.*, vol. 86, no. 2, pp. 414–439, 1990.
[3] R. Coifman, V. Rokhlin, and S. Wandzura, "The fast multipole method for the wave equation: A pedestrian prescription," *IEEE Antennas Propag. Mag.*, vol. 35, no. 3, pp. 7–12, Jun. 1993.
[4] C. C. Lu and W. C. Chew, "A multilevel algorithm for solving a boundary integral equation of wave scattering," *Microw. Opt. Tech. Lett.*, vol. 7, no. 10, pp. 456–461, Jul. 1994.
[5] J. M. Song and W. C. Chew, "Multilevel fast multipole algorithm for solving combined field integral equation of electromagnetic scattering," *Microw. Opt. Tech. Lett.*, vol. 10, no. 1, pp. 14–19, Sep. 1995.
[6] E. Bleszynski, M. Bleszynski, and T. Jaroszewicz, "AIM: Adaptive integral method for solving large-scale electromagnetic scattering and radiation problems," *Radio Sci.*, vol. 31, no. 5, pp. 1225–1251, May 1996.
[7] C. F. Wang, F. Ling, and J. M. Jin, "Adaptive integral solution of combined field integral equation," *Microw. Opt. Tech. Lett.*, vol. 19, no. 5, pp. 321–328, Dec. 1998.
[8] J. R. Phillips and J. K. White, "A precorrected-FFT method for electrostatic analysis of complicated 3-D structures," *IEEE Trans. Comput. Aided Des. Integr. Circuits Syst.*, vol. 16, no. 10, pp. 1059–1072, Oct. 1997.
[9] W. Hackbusch and Z. P. Nowak, "On the fast matrix multiplication in the boundary element method by panel clustering," *Numer. Math.*, vol. 54, pp. 463–491, 1989.
[10] K. Zhao, M. N. Vouvakis, and J.-F. Lee, "Application of the multilevel adaptive cross-approximation on ground plane designs," in *IEEE Int. Symp. Electromagnetic Compatibility*, Santa Clara, CA, 2004, pp. 124–127.
[11] ——, "The multilevel adaptive cross-approximation algorithm for modeling electromagnetic radiation and scattering problems," *PIERs*, Nanjing, China, Aug. 2004.
[12] M. Bebendorf, "Approximation of boundary element matrices," *Numer. Math.*, vol. 86, no. 4, pp. 565–589, Jun. 2000.
[13] S. Kurz, O. Rain, and S. Rjasanow, "The adaptive cross-approximation technique for the 3-D boundary element method," *IEEE Trans. Magn.*, vol. 38, no. 2, pp. 421–424, Mar. 2002.
[14] M. Bebendorf and S. Rjasanow, "Adaptive low-rank approximation of collocation matrices," *Computing*, vol. 70, no. 1, pp. 1–24, Mar. 2003.

[15] S. M. Rao, D. R. Wilton, and A. W. Glisson, "Electromagnetic scattering by surfaces of arbitrary shape," *IEEE Trans. Antennas Propag.*, vol. 30, no. 5, pp. 409–418, May 1982.
[16] E. Michielssen and A. Boag, "A multilevel matrix decomposition algorithm for analyzing scattering from large structures," *IEEE Trans. Antennas Propag.*, vol. 44, no. 8, pp. 1086–1093, Aug. 1996.
[17] J. M. Rius, J. Parron, E. Ubeda, and J. R. Mosig, "Multilevel matrix decomposition for analysis of electrically large electromagnetic problems in 3-D," *Microw. Opt. Tech. Lett.*, vol. 22, no. 3, pp. 177–182, Aug. 1999.
[18] J. Parron, J. M. Rius, and J. R. Mosig, "Application of the multilevel matrix decomposition algorithm for the frequency analysis of large microstrip antenna array," *IEEE Trans. Magn.*, vol. 38, no. 2, pp. 721–724, Mar. 2002.
[19] J. Parron, J. Romeu, J. M. Rius, and J. R. Mosig, "Method of moments enhancement technique for the analysis of Sierpinski pre-fractal antennas," *IEEE. Trans. Antennas Propag.*, vol. 51, no. 8, pp. 1872–1876, Aug. 2003.
[20] A. Breuer, P. Borderies, and J.-R. Poirier, "A multilevel implementation of the QR compression for method of moments," *IEEE Trans. Antennas Propag.*, vol. 51, no. 9, pp. 2520–2522, Sep. 2003.
[21] F. X. Canning and K. Rogovin, "Fast direct solution of standard moment-method matrices," *IEEE Antennas Propag. Mag.*, vol. 40, no. 3, pp. 15–26, Jun. 1998.
[22] S. Kapur and D. E. Long, "IES^3: A fast integral equation solver for efficient 3-dimensional extraction," in *Proc. ICCAD*, 1997, pp. 448–455.
[23] D. Gope and V. Jandhyala, "Oct-tree-based multilevel low-rank decomposition algorithm for rapid 3-D parasitic extraction," *IEEE Trans. Comput. Aided Design Integr. Circuits Syst.*, vol. 23, no. 11, pp. 1575–1580, Nov. 2004.
[24] L. Tsang and Q. Li, "Wave scattering with UV multilevel partitioning method for volume scattering by discrete scatters," *Microw. Opt. Tech. Lett.*, vol. 41, no. 5, pp. 354–361, Jun. 2004.
[25] R. Burkholder and J. F. Lee, "Fast dual MGS block-factorization algorithm for dense MoM matrices," *IEEE Trans. Antennas Propag.*, vol. 52, no. 7, pp. 1693–1699, Jul. 2004.
[26] N. A. Ozdemir and J. F. Lee, "A low rank IE-QR algorithm for matrix compression in volume integral equations," *IEEE Trans. Magn.*, vol. 40, no. 2, pp. 1017–1020, Mar. 2004.
[27] S. M. Seo and J.-F. Lee, "A single-level low rank IE-QR algorithm for PEC scattering problems using EFIE formulation," *IEEE Trans. Antennas Propag.*, vol. 52, no. 8, pp. 2141–2146, Aug. 2004.
[28] K. Zhao and J.-F. Lee, "A single-level dual rank IE-QR algorithm to model large microstrip antenna arrays," *IEEE. Trans. Antennas Propag.*, vol. 52, no. 10, pp. 2580–2585, Oct. 2004.
[29] G. H. Golub and C. F. Van Loan, *Matrix Computations*. Baltimore, MD: The John Hopkins Univ. Press, 1996.
[30] R. F. Harrington, *Field Computation by Moment Methods*. New York: MacMillan, 1968.
[31] M. N. Vouvakis, S.-C. Lee, K. Zhao, and J.-F. Lee, "A symmetric FEM-IE formulation with a single-level IE-QR algorithm for solving electromagnetic radiation and scattering problems," *IEEE Trans. Antennas Propag.*, vol. 52, no. 11, pp. 3060–3070, Nov. 2004.
[32] A. F. Peterson, "The 'interior resonance' problem associated with surface integral equations of electromagnetics: numerical consequences and a survey of remedies," *Electromagnetics*, vol. 10, no. 3, pp. 293–312, Jul./Sep. 1990.
[33] A. F. Peterson, S. L. Ray, and R. Mittra, *Computational Methods for Electromagnetics*. Piscataway, NJ: IEEE Press, 1998.
[34] Y. Saad and M. H. Schultz, "GMRES: A generalized minimal residual algorithm for solving nonsymmetric linear systems," *SIAM J. Sci. Stat. Comput.*, vol. 7, no. 3, pp. 856–869, Jul. 1986.
[35] J.-F. Lee, R. Lee, and R. Burkholder, "Loop star basis functions and a robust preconditioner for EFIE scattering problems," *IEEE Trans. Antennas Propag.*, vol. 51, no. 8, pp. 1855–1863, Aug. 2003.
[36] M. Bebendorf, "Hierarchical LU decomposition based preconditioner for BEM," preprint.
[37] C. L. Holloway, P. McKenna, and R. F. German, "On the application of computational electromagnetic techniques to the design of chambers for EMC compliance testing," *Compliance Eng.*, vol. 2, pp. 19–33, Mar./Apr. 1994.
[38] I. J. Gupta, W. D. Burnside, J.-F. Lee, and R. C. Flibbo, "A novel structure for accurate measurement of antennas mounted on ground plane," in *Proc. 25th Annu. Meeting and Symp.*, Irvine, CA: Antenna Measurement Technique Association, 2003.
[39] R. F. Harrington, *Time Harmonic Electromagnetic Fields*. New York: McGraw-Hill, 1961.
[40] E. S. Siah, K. Sertel, J. L. Volakis, V. V. Liepa, and R. Wiese, "Coupling studies and shielding techniques for electromagnetic penetration through apertures on complex cavities and vehicular platforms," *IEEE Trans. Electromagn. Compat.*, vol. 45, no. 2, pp. 245–256, May 2003.
[41] S. M. Seo and J.-F. Lee, "A fast IE-FFT algorithm for solving PEC scattering problems," *IEEE Trans. Magn.*, vol. 41, no. 5, pp. 1476–1479, May 2005.
[42] C. F. Wang, F. Ling, and J. M. Jin, "A fast full-wave analysis of scattering and radiation from large finite arrays of microstrip antennas," *IEEE Trans. Antennas Propag.*, vol. 46, no. 10, pp. 1467–1474, Oct. 1998.

Kezhong Zhao (S'00) was born in Fujian, China. He received the B.S. (*Summa Cum Laude*) and M.S. degrees in electrical engineering from The O hio State University, in September 2001 and March 2003, respectively. He is currently working toward his Ph.D.

Since September 2001, he has been a Graduate Research Associate in the ElectroScience Lab, Department of Electrical Engineering, The Ohio State University. His research interests include fast integral equation methods, hybrid FEM-BEM methods, domain decomposition methods, and time domain finite element methods.

Marinos Vouvakis (S'99) was born in Agios Nikolaos, Crete, Greece in February 1977. He received the Diploma degree in electrical engineering, from Democritus University of Thrace (DUTH), Xanthi, Greece, in 1999. In the Fall of 1999, he joined the Telecommunications Research Center at Arizona State University as a Graduate Research Assistant. In 2001 he received the M.S. degree from Arizona State University, Tempe, AZ. He is currently pursuing the Ph.D. degree in electrical engineering on an ANSOFT Corporation fellowship at The Ohio State University, Columbus, OH.

He has been a Graduate Research Associate with the ElectroScience Laboratory at The Ohio State University since 2002. His research interests include domain decomposition methods and finite element and integral equation methods.

Jin-Fa Lee (M'74–SM'90–F'04) received the B.S. degree from National Taiwan University, in 1982, and the M.S. and Ph.D. degrees from Carnegie-Mellon University in 1986 and 1989, respectively, all in electrical engineering.

From 1988 to 1990, he was with ANSOFT Corporation, where he developed several CAD/CAE finite element programs for modeling 3-D microwave and millimeter-wave circuits. From 1990 to 1991, he was a post-doctoral fellow at the University of Illinois at Urbana-Champaign. From 1991 to 2000, he was with Department of Electrical and Computer Engineering, Worcester Polytechnic Institute. Currently, he is a Professor at ElectroScience Laboratory, Department of Electrical Engineering, Ohio State University, Columbus. His research interests focus mainly on numerical methods and their applications to computational electromagnetics. His current research projects include analyses of numerical methods, fast finite element methods, fast integral equation methods, hybrid methods, three-dimensional mesh generation, domain decomposition methods, cement finite elements, and finite element tearing and interconnecting methods.